ACS MEASUREMENT SCIENCE Au
AN OPEN ACCESS JOURNAL OF THE AMERICAN CHEMICAL SOCIETY

pubs.acs.org/measureau Article

Plasma-Droplet Reaction Systems: A Direct Mass Spectrometry Approach for Enhanced Characterization of Lipids at Multiple Isomer Levels

Alexander J. Grooms, Anna N. Nordmann, and Abraham K. Badu-Tawiah*

Cite This: *ACS Meas. Sci. Au* 2023, 3, 32−44 Read Online

ABSTRACT: Neutral triacylglyceride (TG) lipids are critical in cellular function, signaling, and energy storage. Multiple molecular pathways control TG structure via nonselective routes making them structurally complex and analytically challenging to characterize. The presence of C=C bond positional isomers exacerbates this challenge as complete structural elucidation is not possible by conventional tandem mass spectrometric methods such as collision-induced dissociation (CID), alone. Herein, we report a custom-made coaxial contained-electrospray ionization (ESI) emitter that allows the fusion of plasma discharge with charged microdroplets during electrospray (ES). Etched capillaries were incorporated into this contained-ES emitter, facilitating the generation of reactive oxygen species (ROS) at low (3 kV) ESI voltages and allowing stable ESI ion signal to be achieved at an unprecedented high (7 kV) spray voltage. The analytical utility of inducing plasma discharge during electrospray was investigated using online ionization of neutral TGs, *in situ* epoxidation of unsaturation sites, and C=C bond localization via conventional CID mass spectrometry. Collisional activation of the lipid epoxide generated during the online plasma-droplet fusion experiment resulted in a novel fragmentation pattern that showed a quadruplet of diagnostic ions for confident assignment of C=C bond positions and subsequent isomer differentiation. This phenomenon enabled the identification of a novel TG lipid, composed of conjugated linoleic acid, that is isomeric with two other TG lipids naturally found in extra virgin olive oil. To validate our findings, we analyzed various standards of TG lipids, including triolein, trilinolein, and trilinolenin, and isomeric mixtures in the positive-ion mode, each of which produced the expected quadruplet diagnostic fragment ions. Further validation was obtained by analyzing standards of free fatty acids expected from the hydrolysis of the TG lipids in the negative-ion mode, together with isomeric mixtures. The chemistry governing the gas-phase fragmentation of the lipid epoxides was carefully elucidated for each TG lipid analyzed. This comprehensive shotgun lipidomic approach has the potential to impact biomedical research since it can be accomplished on readily available mass spectrometers without the need for instrument modification.

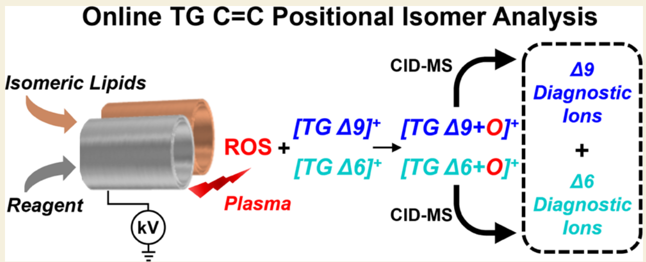

KEYWORDS: *mass spectrometry, lipid isomers, analytical methods, double-bond localization, electrospray ionization*

■ INTRODUCTION

An active goal in lipidomics is to increase the number and type of lipid species identifiable in a given biological system.[1−3] Recent advances in mass spectrometry (MS) have accelerated the field toward this goal; however, the great structural complexity within the lipidome resultant from environmental, pathological, and physiological conditions makes analysis challenging.[3,4] The presence of neutral and isomeric lipid species present a heightened challenge that MS alone cannot address as mass spectrometers mainly measure the mass-to-charge (m/z) ratio of analytes.[1,5] Overcoming this challenge is important as lipid structure—including polarity, charge, and degree of unsaturation—alters biological function.[6−8] Triglyceride (TG) lipids are one such class of lipids that have been historically challenging for MS analysis[9−11] due to the lack of charge carrying group and high potential for isomeric species within the three acyl chain constituents attached to the glycerol head group.

TGs act as energy storage repositories in adipose tissue, hydrolyzing via hormone-sensitive enzymes (e.g., lipase) to give free fatty acids (FAs) for normal physiological function.[12,13] The two major de novo pathways for TG biosynthesis are the Kennedy pathway[14] and the monoacylglycerol pathway,[15] which both utilize fatty acyl-CoAs synthesized by acyl-CoA synthases for acyl chain construc-

Received: July 27, 2022
Revised: September 15, 2022
Accepted: September 15, 2022
Published: October 18, 2022

https://doi.org/10.1021/acsmeasuresciau.2c00051
ACS Meas. Sci. Au 2023, 3, 32−44

tion.[16] TGs are synthesized via the monoacylglycerol pathway in the small intestine using components of dietary fats, where diacylglycerol and fatty acyl-CoA are covalently bonded to form the TG.[17,18] The excessive buildup of TGs in this manner is associated with human metabolic syndrome, which includes diabetes, heart disease, obesity, and stroke.[19−22] The excess accumulation and subsequent lipase-activated hydrolysis of TGs have been shown to play a critical role in cancer pathogenesis.[23] The β-oxidation of FAs obtained from TGs has been linked to cancer proliferation. The energy provided via FA oxidation has been shown to drive prostate[24] and pancreatic[25] cancers, while β-oxidation inhibition has been shown to promote leukemia and glioblastoma cellular apoptosis.[26,27]

The function of TGs and FA hydrolysis products in metabolic syndrome and cancer is directly related to acyl chain structural complexity. The position of the C=C bond, three carbons from the terminus versus six carbons designates the acyl chain and resultant FFA as omega-3 (ω-3) and omega-6 (ω-6), respectively. The functions of these structurally similar species are vastly different as high ratios of ω-6/ω-3 promote metabolic disease and cancer pathogenesis, whereas lower ratios exhibit suppressive effects of such diseases.[28−32] Cancer cells have also been shown to have altered lipid metabolism, utilizing alternate fatty acid desaturation pathways that yield aliphatic chains with C=C bonds at unusual locations.[33]

The common occurrence of C=C bond positional isomers has prompted the MS-focused lipidomics community to develop analytical tools for the differentiation of these important species. Generally, such efforts can be split into two categories: (i) specialized high-energy (relative to collision-induced dissociation (CID)) tandem MS methods and (ii) innovations in derivatization and ionization techniques prior to MS introduction. High-energy tandem MS methods include ozone-induced dissociation using a modified linear ion trap MS,[34−36] electron impact excitation of ions from organics (EIEIO) using a modified electron capture dissociation (ECD) cell for high-energy electron production,[37] and 193 nm ultraviolet photodissociation (UVPD) utilizing a modified orbitrap MS.[38] Long reaction and spectral acquisition times limit the above methods when high-throughput workflows are desired. Additionally, these methods have been limited to few academic laboratories, necessitating the development of methods that can utilize the conventional CID tandem MS approach that is widely available on almost all commercial mass spectrometers. In this case, unique front-end derivatization and ionization techniques have been employed for C=C bond localization. Such techniques include the Paternò−Büchi reaction which utilizes UV irradiation of acetone followed by ionization and CID tandem MS to give fragment ions diagnostic to the C=C bond location.[39−43] This reaction has been performed in bulk and online for lipids and FA isomer differentiation. However, it suffers from low yield when irradiation is on the timescale comparable to that of MS acquisition. Ozone electrospray ionization (OzESI) has been used for the production of diagnostic ions after ozonolysis; however, external ozone generation equipment is needed. The OzESI process produces complex spectra because diagnostic ions appear with molecular ions in full MS (without mass selection) making spectral interpretation difficult.[44] Epoxidation of the C=C bond for characterization of double-bond configuration has gained interest recently and has been performed offline via bulk phase meta-chloroperoxybenzoic acid (m-CPBA) epoxidation[45] and via the use of reactive oxygen species (ROS) produced in nonthermal plasma discharge.[46−48] Epoxidation via ROS in nonthermal plasma is of interest because the reaction proceeds fast—on the timescale of MS acquisition, occurs under atmospheric conditions with no added reagents, and produces well-defined, characteristic fragment ions upon subjecting the epoxide ring to CID.

Scheme 1. Schematic Illustration of Structural Information Derived from Positive-Ion Mode Analysis of TGs and Negative-Ion Mode Analysis of FAs via (A) Conventional ESI Providing Only Side Chain and Head Group Information, Respectively, upon CID, and (B) Contained-ESI Capable of Plasma-Droplet Fusion Where the Combination of ROS Reactions and CID Yield Multiple Level of Isomer Differentiation, Including Head Group, Side Chain, and C=C Positional Isomers

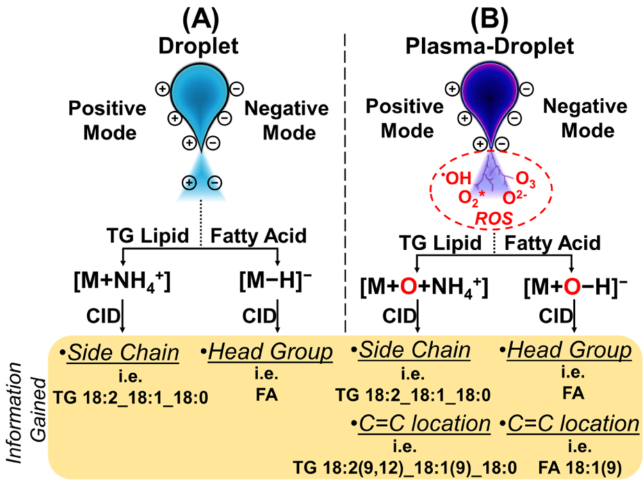

Herein, we employ the phenomenon of generating ROS from nonthermal plasmas in a novel coaxial contained-electrospray (ES) experiment that fuses plasma and charged droplets together for online ionization, epoxidation, and the localization of double bonds in unsaturated TG lipids in complex mixtures. Traditionally, electrospray ionization (ESI) and nonthermal plasma discharge are separate and incompatible physical processes. However, recent fundamental work has demonstrated that the two processes can coexist, dependent on the emitter type and spray conditions.[49] Chemically etched silica capillaries are one such emitter type that we find facilitates concurrent ES and plasma formation. The mechanism of this phenomenon is the topic of an ongoing fundamental study. However, we suggest the etched silica capillaries facilitate plasma formation due to their physical properties including surface roughness, wettability, conductivity, and sharpness of the emitter tip produced via etching. We hypothesize that super reactive and analytically useful charged microdroplets can be created at low (3 kV) onset voltages by fusing the ROS species from etched silica capillaries with microdroplets generated from conventional ESI in a contained setup.[50−53] That is, the nonthermal discharge (plasma) from the etched capillary is allowed to mix (fuse) with charged droplets generated from a deactivated fused silica capillary in real time by spraying the two separate capillaries coaxially into a small cavity that is included into the contained-ES ion source.

https://doi.org/10.1021/acsmeasuresciau.2c00051
ACS Meas. Sci. Au 2023, 3, 32−44

The resultant plasma-droplet system (Scheme 1B) is coupled with MS to characterize isomers of TG lipids and FAs without prior separation, derivatization, or modification of the existing mass spectrometer. Specifically, we have used this new experimental setup to distinguish C=C positional isomers in mixtures of TGs in positive-ion mode. We then applied the method to directly analyze extra virgin olive oil (EVOO), in which two new acyl chain and positional isomers of a TG were identified and characterized for the first time. We validated our findings with negative-ion mode analysis of EVOO where FAs hydrolyzed from the corresponding TGs lipids were characterized. In the absence of nonthermal plasma (Scheme 1A), the conventional ESI-MS/MS yielded only side chain and head group information with no capacity to elucidate C=C bond positional isomers in the mixture.

EXPERIMENTAL SECTION

Creation of Coaxial Contained-Electrospray Emitter

The coaxial contained-electrospray source (Figure 1) for the production of the plasma-droplet reaction system was constructed

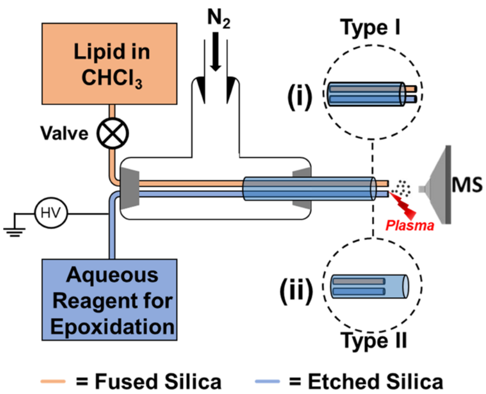

Figure 1. Diagram showing the coaxial contained-ESI emitter for facilitation of plasma-droplet fusion reactions where lipid solution is delivered via deactivated fused silica capillary (orange line) and ammonium acetate solution is sprayed from etched silica (blue line) for in situ generation of ROS. Droplets from the two coaxial spray converge into an outer etched silica capillary. This outlet is operated in two modes: (i) Type I mode in which the inner capillaries protrude from the outer, facilitating droplet-phase reaction on a faster (μs) lifetime and (ii) Type II mode in which the inner capillaries regress into the outer capillary, creating a cavity that facilitates extended reagent mixing in a thin film for subsequent reactions on seconds timescale. The red thunder symbol indicates plasma generation from the etched silica capillary, which interacts with charged droplets from the fused silica.

from a Swagelok cross-junction (see the Supporting Information for details), which allowed three inputs and one configurable outlet. Lipid solution in chloroform (10 μL/min) and ammonium acetate reagent (1 μL/min) was delivered coaxially through a deactivated fused silica capillary (100 μm i.d.) and chemically etched silica capillary (100 μm i.d.), respectively, into the cavity of the outer etched silica capillary (450 μm i.d.). The outer cavity provides an avenue for plasma-droplet mixing and epoxidation reaction before exiting the contained-ESI source. The mixing process and the reactant delivery to the proximal mass spectrometer were assisted by a nitrogen nebulizer gas input (150 psi). As depicted in Figure 1, two operational modes of the contained-ES source are possible: (1) Type I mode operation (Figure 1i) in which the 100 μm i.d. etched capillary protrudes from the outer capillary and (2) Type II mode of operation (Figure 1ii) in which the 100 μm i.d. silica capillaries are recessed ~2 mm into the cavity of the etched 450 μm i.d capillary. Additional experimental details are in the Supporting Information.

RESULTS AND DISCUSSION

The novelty of this work lies in the establishment of a new plasma-droplet reaction system that enabled the electrical energy inherent in electrospray to be harnessed for online epoxidation reactions and to generate stable ion signal for online MS analysis even up to 7 kV of applied direct current (DC), without disturbing mass spectrometer electronics. The contained-ES device that enabled the plasma-droplet reactions was designed with the long-term goal to couple to liquid chromatography (LC)-MS, where it can act as both the ion source and reactor for instantaneous modification of analytes eluting from the LC column. The current report presents direct infusion experiments, applied to derivatize, and analyze TG lipids. Following the initial method optimization, we first discuss positive-ion mode analysis of various standards and isomeric mixtures of TGs. Then, we move on to discuss results of complex mixture analysis, and finally, FA analysis in negative-ion mode using the same plasma-droplet reaction system.

Optimization of the Plasma-Droplet Reaction System

Initial efforts to develop the coaxial contained-ESI source were focused on the optimization of ROS generation during the electrospray process using chemically etched silica capillaries. Although incompatible in traditional ESI,[49] we used etched silica capillaries for concurrent plasma and stable ESI plume formation. Figure S1C,D shows operation of a contained-ESI emitter in Type II mode with deactivated fused silica and etched silica capillaries, respectively. The plasma discharge is observed mainly inside the cavity during electrospray and well separated from the mass spectrometer inlet. We use MS as an indicator for ROS generation via the reaction of C=C bonds to yield the expected epoxide product as evidence for plasma formation. When the breakdown potential of ambient air is met, high-energy electrons collide with atmospheric species yielding ROS consisting of excited-state atomic oxygen, molecular oxygen, and ozone (O_3).[54,55] These species are well known to oxidize C=C bonds to give the epoxide reaction product, indicated by the appearance of a peak at +16 Da away from the expected molecular weight. The fragmentation of the epoxide product provides unique diagnostic ions after CID tandem MS.[56]

We chose oleic acid (MW 282 Da) for the characterization of ROS generation during ESI when using the etched capillary. Oleic acid has a C=C bond at the 9Z position and ionizes readily in negative-ion mode to yield $[M - H]^-$ at m/z 281. When subjected to ROS in plasma, the epoxide product forms giving $[M - H + O]^-$ at m/z 297. Additional products at m/z 313 and 329 can form at higher voltages and have been attributed to the addition of superoxide[57] and ozonide[58] species over the double bond, respectively. These peaks are absent when oleic acid is analyzed using the deactivated fused silica capillary. This data is summarized in Figure 2, where experiments were performed across the range of 2−7 kV spray voltage. The resultant mass spectra in Figure 2A show a steady increase in the epoxide product for the etched silica emitter as spray voltage increased and a null effect for the deactivated fused silica emitter. These data were used to evaluate signal stability versus spray voltage via the total ion chronogram (TIC) for both emitters in Figure 2B. ROS product yield (i.e.,

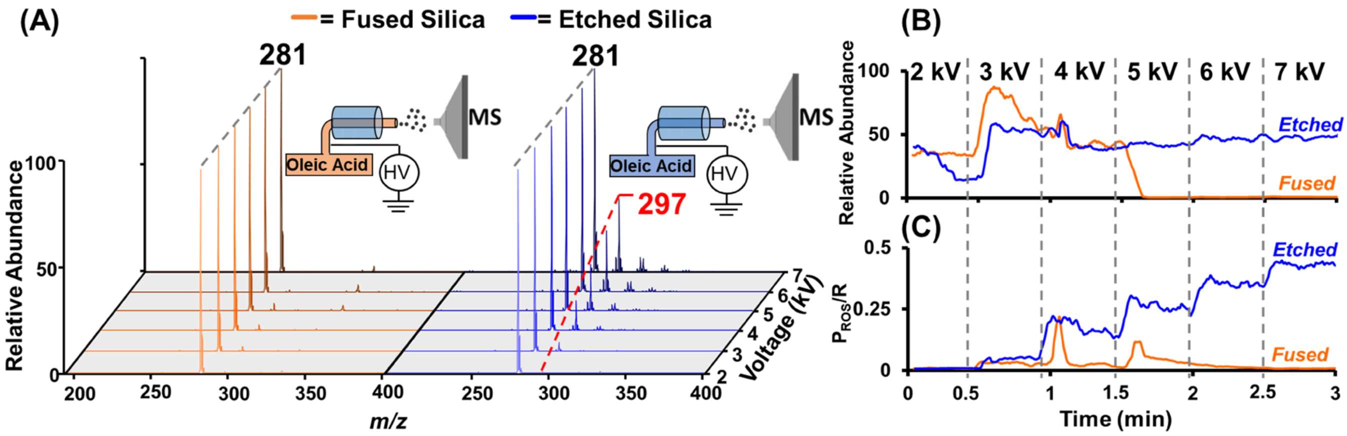

Figure 2. Comparison of conventional deactivated fused silica emitters with chemically etched emitters during: (A) Negative-ion mode MS analysis of oleic acid (MW 282 Da) from conventional deactivated fused silica emitter (orange) and chemically etched silica (blue). The corresponding depiction of the Type I emitter configuration used (insets) shows the effect of spray voltage on epoxide product formation at m/z 297, which is prominent in etched emitter operation. (B) TIC of oleic acid analyses using deactivated fused silica (orange) and etched silica (blue) emitters under identical experimental conditions showing signal stability of the etched emitter versus that of the conventional emitter at varying spray voltage. (C) Plot of ROS reaction yield showing the production of oleic acid oxidation product for deactivated fused silica and etched silica capillaries under identical experimental conditions showing ROS onset formation at 3 kV spray voltage and increased reaction yield with increased spray voltage for the etched silica emitter.

$I_{297} + I_{313}/I_{281}$) was evaluated via the extracted ion chronogram (EIC) at m/z 281, 297, and 313 versus the applied spray voltage as shown in Figure 2C.

Three notable differences are observed between the performance of the deactivated fused silica capillary (orange line in Figure 2) and chemically etched silica capillary (blue line in Figure 2), including: (i) a sharp decrease in signal intensity for the fused silica capillary when spray voltage reached 5 kV (Figure 2B), whereas the etched silica capillary maintained relatively constant signal intensity across the entire range of 2−7 kV; (ii) the etched silica emitter showed a steady increase in ROS production at each voltage interval (Figure 2C) giving approximately 40% ROS yield at 7 kV, yet showing the onset of the ROS at as low as 3 kV; and (iii) the fused silica emitter showed the sporadic formation of ROS with spikes occurring at 4 and 5 kV spray voltages (Figure 2C). The stable signal and the increasing ROS yield (relative to spray voltage) observed for the etched silica capillary are surprising but have been reproduced multiple times on different days (Figure S2). We explain these phenomena, respectively with (i) the loss of signal at high spray voltage with the fused silica capillary is expected due to the inability of Taylor cone formation once discharge has quenched the electric field at the emitter.[49] (ii) Increasing ROS production with voltage using the etched silica emitter, including ROS onset at low (3 kV) spray voltage and stable ESI spray signal at voltages up to 7 kV, is due to etched emitter stabilization of concurrent plasma formation with ESI, whereas (iii) the sporadic ROS onset with the fused emitter is due to an inability to maintain plasma and stable ESI. Such unique properties of the etched silica capillary suggest its use can be a powerful tool for the generation of super reactive droplets containing ROS (Scheme 1B). Although this plasma-droplet system can be used to study many different reactions, we choose to investigate the reaction of ROS with C═C bond in lipid species for the purposes of isomer differentiation. See the Supporting Information (Figure S3) for details on the optimization of experimental parameters (spray voltage, flow rate, and nebulizer gas pressure) that produced maximum C═C bond oxidation.

Analysis of Triacylglyceride Standards

After optimization, we applied the coaxial contained-ES emitter to ionize and localize double-bond positions in unsaturated TGs. Historically, TG analysis via MS alone has been limited due to the lack of an easily ionizable functional group and low solubility in polar solvents, which has called for high-energy and gas-phase ionization techniques including electron impact and fast atom bombardment.[11] Ionization of TGs via ESI has been widely performed via ammonium adduct formation giving rise to $[M + NH_4]^+$ ions, which is particularly useful in LC methods where ammonium is often employed as a cationic buffer ion.[11,59] The coaxial mode of contained-ES allows the potential for ammonium adduct formation and the use of ESI unfriendly solvents (e.g., chloroform) by fusing/mixing droplets from a capillary containing TG analyte in chloroform and another containing aqueous phase ammonium acetate. We observe a similar increase in absolute intensity via ammonium adducts of TGs in this direct infusion experiment as in analogous LC methods.[60] Our development of contained-ES ion sources is ongoing,[50,51] with recent studies highlighting the power of coaxial mode to facilitate online charged microdroplet reactions from liquid phase reagents introduced individually to the configurable output of the emitter.[61,62] Spray dynamic studies using emitters similar to the Type I mode (Figure 1i) of the contained-ES (i.e., in the absence of reaction cavity), showed droplet speed is on the order of 100 m/s at >100 psi N_2 pressure.[63,64] At 1 mm spray distance (emitter tip to MS inlet), droplet lifetime is on the microseconds timescale suggesting nonequilibrium mixing of reagent droplets. In Type II mode (Figure 1ii), however, the presence of a cavity allows coalescence of the initial microdroplets to form bulky secondary droplets (∼25 μm) that move slowly (∼10 mm/s) among a thin film formed on the inner walls of the outer capillary. Thus, droplet lifetime is controllable by the size of the cavity (determined by the extent to which the inner capillaries are recessed) and the N_2 nebulizer gas pressure.[51] The addition of etched capillaries to the coaxial contained-ES emitter adds a second dimension of complexity, which is presented in this work for the first time.

https://doi.org/10.1021/acsmeasuresciau.2c00051
ACS Meas. Sci. Au 2023, 3, 32−44

All TG studies were performed in the presence of cavity (i.e., Type II configuration) as comparative experiments with Type I mode did not yield desired TG adducts (Figure S4). A 2 mm cavity size provided optimal adduct formation (Figure S5). This is attributed to the necessity of turbulent mixing and adequate interaction time between the TG and the adduct-forming reagent.

Extensive emitter optimization experiments using TG 18:1(9Z)/18:1(9Z)/18:1(9Z) (triolein, MW 885 Da) were performed and may be seen in Figures S6, S7, S8, and S9 along with discussion in the Supporting Information.

Epoxide formation by the plasma-droplet fusing reaction allows isomeric species of lipids to be distinguished when subjected to MS/MS. For free fatty acids, the distinct fragmentation of the epoxide ring has been widely discussed (Scheme S1), which is known to give two diagnostic ions that are 16 Da apart signaling the specific location of a C═C bond along the carbon chain.[48,57] We have observed a novel fragmentation pattern for epoxides derived from TG lipids. Scheme 2 provides a cartoon depiction of the MS/MS process for generating quadruplet diagnostic ions for a TG with a single double bond (Scheme 2A) and TG with two double bonds (Scheme 2B) along the acyl chains. For a TG molecule with one C═C bond in each of the side chains, the collision-induced fragmentation gives the lyso form, which subsequently dissociates to afford two more diagnostic ions (in addition to those originating from the intact lipid). Thus, we obtain four total diagnostic ions per double bond in TG lipids. For TG lipids with two double bonds along the side chains, we detect both a single epoxide (+O) and double epoxide (+2O) reaction products in the plasma-droplet experiment. We found that the identification of the positions of both C═C bond can be achieved more readily when the MS/MS of both the +O and +2O epoxide products are considered, as illustrated in Scheme 2B. A detailed mechanism of this insight is provided in Schemes S2−S4. This capability is showcased below using the analysis of standards of mono- and poly-unsaturated lipids, including isomeric counterparts.

Scheme 2. Schematic Showing Ionization (NH_4^+ Adduct), Epoxidation, and CID of (A) TG Lipid with a Single C═C Bond Side Chain to Give Four Diagnostic Ions Per Double Bond: Two from Dissociation of Intact Lipid, and Two from Cleavage of the Lyso Form of the Lipid, (B) TG with a Two Double-Bond Side Chain Demonstrating the Importance of Analyzing MS/MS for Both the Single (+O) and Double (+2O) Epoxidation Products for Complete C═C Position Assignments for both Double Bonds

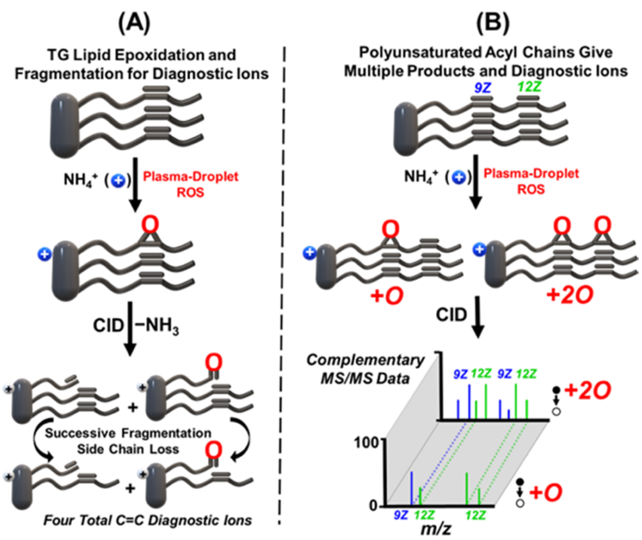

Here, we applied the epoxide fragmentation pattern to four (4) selected TG lipids to evaluate the double-bond configurations (Figure 3): triolein and its C═C positional isomer TG 18:1(6Z)/18:1(6Z)/18:1(6Z), trilinolein, and trilinolenin. We begin with discussion evaluating triolein under plasma-droplet fusing conditions. The full MS in Figure 3A shows the base peak ammonium adduct of triolein at m/z 903 with the epoxide product at m/z 919. The inset MS/MS of the triolein epoxide product shows the expected diagnostic ions related to a C═C bond at the 9Z position obtained after CID. Diagnostic ions ***1*** and ***2*** correspond to the expected epoxide fragmentation of the lyso product of triolein after losing one oleic acid side chain, whereas diagnostic ions **3** and **4** correspond to the expected epoxide fragmentation of the intact lipid as displayed in Figure 3B. The complete fragmentation scheme with expected diagnostic ions is summarized in Scheme S2. The inset MS/MS in Figure 3A also shows the expected neutral loss of oleic acid with the addition of a peak at +16 Da at m/z 620, attributed to the epoxide product lyso-form. Other MS/MS fragments are observed such as the NH_3 neutral loss to give ion at m/z 903, followed by a sequential water loss to give the ion at m/z 884 as explained in Figure S9A.

Figure 3C shows full MS recorded when the 6Z positional isomer of triolein was subjected to the plasma-droplet fusing reactions on the contained-ESI source. High-abundant ions derived from ammonium adduction are observed at m/z 903, alongside the epoxidation product at m/z 919. The inset in Figure 3C shows MS/MS of the epoxide product. Diagnostic ions **5** and **6** correspond to the expected epoxide fragmentation of the lyso product of the 6Z isomer after losing one side chain, whereas diagnostic ions ***7*** and ***8*** correspond to the expected epoxide fragmentation of the intact lipid as summarized in Figure 3D. The complete mechanistic scheme leading to the fragmentation of C═C to give the observed quadruplet diagnostic ions is shown in Scheme S3.

The complexity of the lipid analyte was increased from mono-unsaturation in triolein (18:1) to poly-unsaturation in trilinolein (18:2), where there are two C═C bonds located at the 9Z and 12Z positions. Figure 3E shows the full MS recorded when trilinolein (MW 879 Da) was analyzed using the contained-ES source under the plasma-droplet reaction condition. The ammonium adduct of trilinolein was observed at m/z 897, alongside multiple epoxidation products including the single (+O) and double (+2O) epoxidation products at m/z 913 and 929, respectively. All 9Z and 12Z positions on the three acyl chains of trilinolein are chemically equivalent, thus these epoxidations may occur at any of these sites. Assuming a statistical distribution of ROS epoxidation at all of the available C═C sites, we acknowledge that superoxide addition can contribute to the double epoxide product at m/z 929. However, we suggest that the double epoxide product has a significant contribution to the +32 Da peak at m/z 929, which is from the simultaneous oxidation at the 9Z and 12Z locations.

This interpretation is supported by the MS/MS shown in the inset of Figure 3E where blue fragments (m/z 475, 491, 754, and 772) correspond to the fragmentation of the epoxide

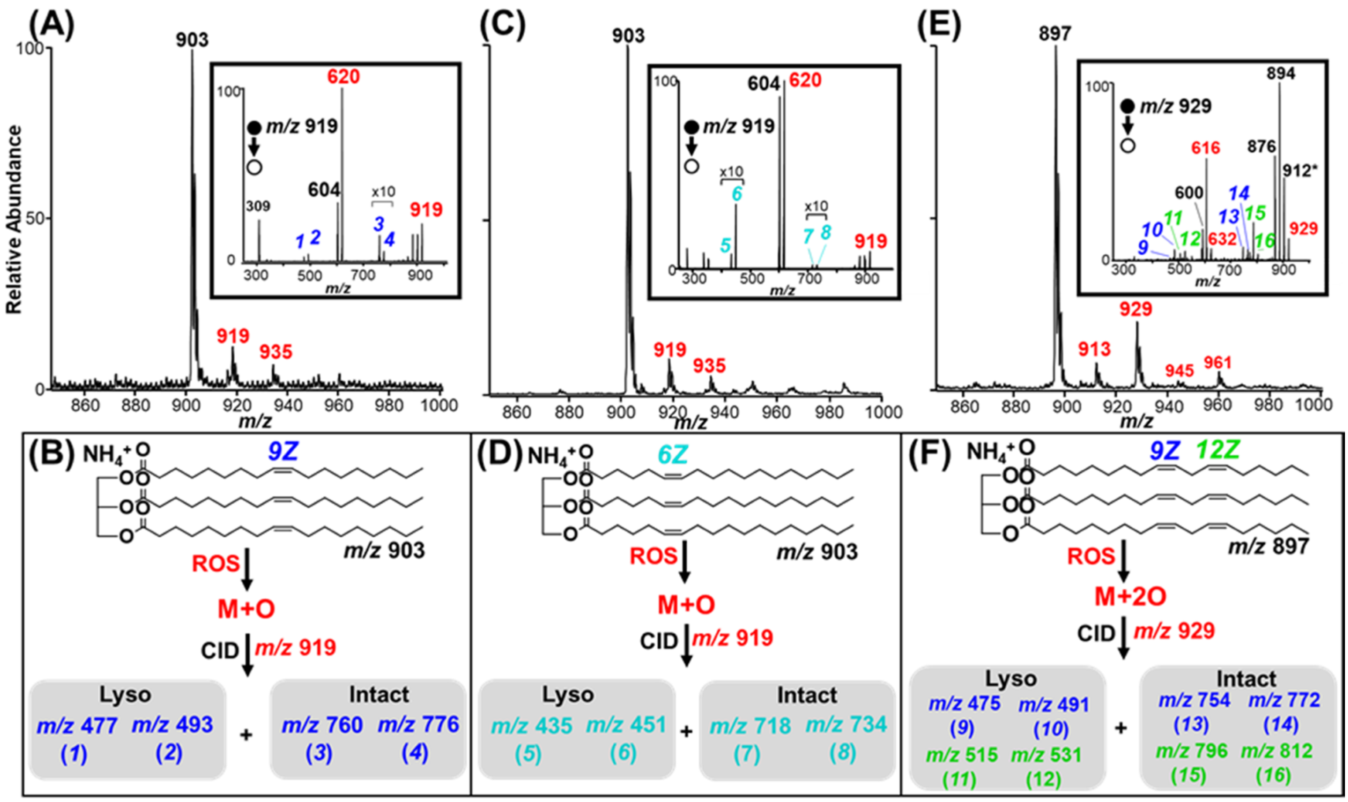

Figure 3. Positive-ion mode MS analysis of TGs via plasma-droplet fusing reactions: (A) full mass spectrum of triolein, with ammonium adduct at m/z 903. Inset MS/MS shows CID of the single epoxide product at m/z 919 giving 9Z C═C bond diagnostic ions ***1***, ***2***, ***3***, and ***4***. (B) Reaction scheme illustrating how the diagnostic ions are related to the lyso and intact triolein after fragmentation of the epoxide ion at m/z 919; (C) full mass spectrum of triolein isomer with 18:1 (6Z) side chains with the inset MS/MS showing CID of the single epoxide product where diagnostic ion ***5***, ***6***, ***7***, and ***8*** are detected. (D) Reaction scheme illustrating the relationship between diagnostic ions derived from lyso and intact form of the triolein isomer; (E) full mass spectrum of trilinolein, with ammonium adduct at m/z 897 and the corresponding epoxide products at intervals of 16 Da. Inset: MS/MS showing CID of the double epoxide product at m/z 929 giving 9Z diagnostic ions (***9***)/(***10***) and (***13***)/(***14***), along with 12Z diagnostic ions (***11***)/(***12***) and (***15***)/(***16***). (F) Reaction scheme showing the formation of the double epoxide product at m/z 929 with subsequent production of four MS/MS diagnostic ions for the 9Z position (blue) and four diagnostic ions for the 12Z position (green).

at the 9Z location and green fragments (m/z 515, 531, 796, 812) correspond to the dissociation of epoxide at the 12Z position, as summarized in Figure 3F. All expected diagnostic ions, including those from the lyso-form of trilinolein, are observed in the tandem mass spectrum supporting the use of this method for double-bond localization. Tandem data of m/z 913, corresponding to the single epoxidation product is shown in Figure S10A. As discussed in Scheme 2B, we emphasize the importance of evaluating the tandem MS of both the single and double epoxidation products to achieve a full picture of all possible diagnostic ions. Diagnostic ions for both the 9Z and 12Z sites are present, supporting the above classification. However, not all eight expected fragments could be identified for the single epoxide peak, suggesting the use of the double epoxide product for structural information is more efficient. An additional interesting observation in Figure S10A is that two of the ions corresponding to the 9Z position were observed at 2 Da less than expected. This may be attributed to the loss of H_2 via dehydrogenation during CID fragmentation. Additional evidence of dehydrogenation is shown in Figure S10B, where the lyso ion region from m/z 590−640 and precursor ion region from m/z 860−940 of the double epoxide products are clearly shown. The loss of NH_3 from the precursor at m/z 929 is seen at m/z 912 along with a peak at 2 Da lower suggesting sequential H_2 loss. Two water loss events are also observed for the double epoxide product in contrast to the one water loss peak observed in the single epoxidation product. In the zoomed-in lyso region of Figure S10B, the expected lyso product ion is observed at m/z 600 alongside two sequential −2 Da peaks attributed to dehydrogenation. Likewise, the single and double epoxidation lyso product ions are observed at m/z 616 and 632 respectively, with dehydrogenation peaks at −2 Da for each. A complete fragmentation scheme for trilinolein with all expected diagnostic ions is summarized in Scheme S4.

Like the other lipids, the full mass spectrum for trilinolein showed additional peaks that are +16 Da apart, besides the single and double epoxidation peaks. In this case, we believe the additional peaks at m/z 945 and 961 are likely due to multiple superoxide additions and/or further epoxidation products on the other linoleic acyl chains. Since the epoxidation reaction is a nonspecific process, we need at least one of these peaks to make C═C position assignment, although the full picture emerges if more than one epoxide is considered especially for poly-unsaturated TGs. Interestingly, these additional peaks provide some indication of the number of double bonds in the lipid, with triolein (one C═C bond) trilinolein (two C═C bonds), and trilinolenin (three C═C bonds) showing two, four, and six epoxide/superoxide peaks, respectively.

The last, and most structurally complex standard lipid evaluated was trilinolenin, which is a poly-unsaturated TG

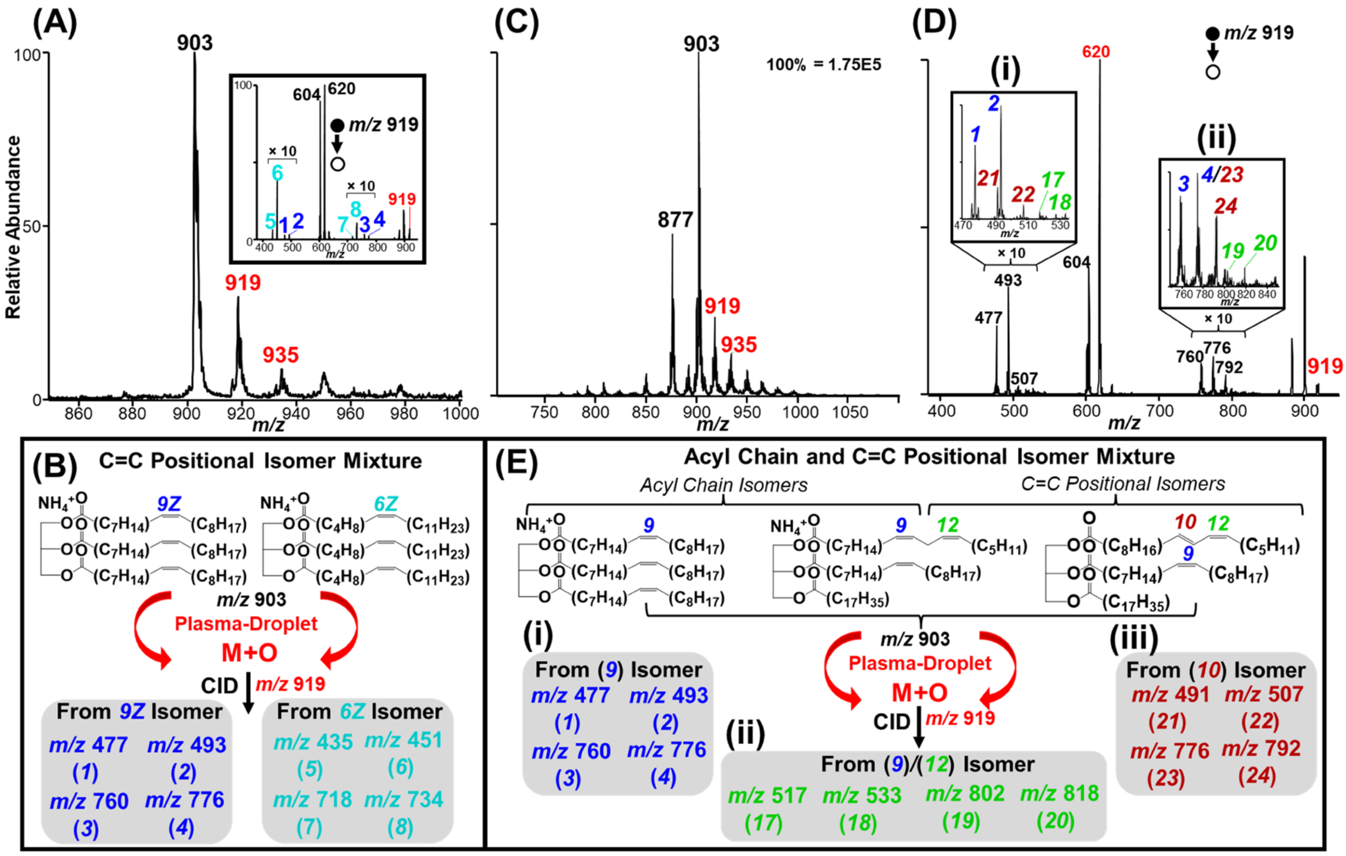

Figure 4. Positive-ion mode MS analysis of isomeric standard TG and complex olive oil samples. (A) Full mass spectrum of a mixture of two standard TGs isomers, one containing oleic acid (18:1, 9Z) side chains and another containing 18:1(6Z) side chains. The epoxide lipids were both observed at m/z 919, with the inset tandem MS showing expected quadruplet diagnostic ions for the 9Z and the 6Z positions, as fully described in (B). (C) Full mass spectrum of EVOO under plasma-droplet fusing conditions. (D) MS/MS of the epoxide peak at m/z 919 in (C), where inset (i) shows zoomed-in mass range for the lyso-form diagnostic ions and inset (ii) shows zoomed-in mass range for the intact form revealing the diagnostic ions that correspond to the presence of three isomeric TG lipids: TG 18:1(9)/18:1(9)/18:1(9), TG 18:2(9,12)_18:1(9)_18:0, and TG 18:2(10,12)_18:1(9)_18:0. The structures of these three TG isomers detected in EVOO are provided in (E) as well as their corresponding diagnostic ions in the groups of (i), (ii), and (iii) for the three TG isomers.

(18:3) with three double bonds at the 9Z, 12Z, and 15Z locations on each linolenic side chain. The full mass spectrum and associated MS/MS of the single, double, and triple epoxide products are displayed in Figure S11, along with a discussion of the expected spectral features. All 12 expected diagnostic fragments ions for trilinolenin are summarized in Scheme S5. Again, we emphasize the importance of evaluating the tandem MS of each epoxide product to obtain the full picture of all 12 diagnostic ions; for trilinolenin the task of identifying all expected fragment ions becomes extremely difficult without considering the contribution from each MS/MS data. In sum, we observed all expected diagnostic ions based on the breadth of the three MS/MS epoxidation products and these (expected and observed ions) are summarized in Table S1 for all four standard TG lipids tested.

Differentiation of Isomeric TG Standard Mixtures

After determining that the plasma-droplet reaction system can be applied to localize C═C bond positions in selected TG lipids, we aimed to evaluate the emitter's capability to perform isomeric and complex mixture analysis. First, we discuss the isomeric mixture analysis (Figure 4A,B), which involved a mixture of triolein with 9Z double bonds together with its C═C positional isomer with 6Z double bonds. Figure 4A shows the mass spectrum of the mixture sprayed under plasma-droplet fusing conditions. As expected, the isomers give identical pseudomolecular ions at m/z 903 corresponding to the lipid ammonium adduct with the single epoxide product at m/z 919 as well as the over-oxidized product at m/z 935. The inset tandem MS data in Figure 4A shows diagnostic ions ***1*** and ***2*** alongside ***5*** and ***6*** corresponding to the lyso-form diagnostic ions of triolein (i.e., 18:1(9Z) side chains) and the 18:1(6Z) side chain isomer, respectively. Additionally, the diagnostic ions ***3*** and ***4*** appear alongside ***7*** and ***8*** corresponding to diagnostic ions of the intact form of triolein and the 18:1(6Z) side chain isomer, respectively. A schematic representation of the epoxidation process, followed by fragmentation of the isomers to achieve the expected diagnostic ions is shown in Figure 4B. This result demonstrates the power of the plasma-droplet reaction system to enable the traditional CID process to differentiate positional isomers of TG lipids without prior separation or instrument modification. This capability was further explored by analyzing untreated extra virgin olive oil (EVOO) sample, which is known to contain various levels of isomeric lipid species, including acyl chain and positional isomers.

Analysis of EVOO Complex Mixture

The contained-ES platform with novel plasma-droplet reaction capabilities was tested in its ability to perform complex mixture

https://doi.org/10.1021/acsmeasuresciau.2c00051
ACS Meas. Sci. Au 2023, 3, 32−44

analysis. We used EVOO samples that were diluted 1000×. Because of its rich lipid and FFA content, EVOO has been the subject of lipidomics analysis in food science, especially studies related to adulteration of this important oil.[65,66] The most abundant TG in EVOO has been defined as TG 18:1(9)/18:1(9)/18:1(9).[66] Prior studies suggest,[66] however, that an acyl chain isomer of this TG may also be a component of EVOO. The lipid TG 18:2(9,12)_18:1(9)_18:0 yields the same molecular weight of 885 Da as the abundant TG. Although this isomer was suggested,[66] the authors were unable to distinguish the isomers using conventional direct infusion ESI of diluted EVOO samples.

Here, we evaluate the presence of this acyl chain isomer and provide evidence for the existence of additional TG C=C positional isomers that have not been previously reported. Figure 4C shows the positive-ion mode full mass spectrum of the diluted EVOO sample. The base peak in the spectrum occurs at m/z 903 which is analogous to triolein ammonium adduct. However, we suggest there is contribution to this peak from the ammonium adduct of the isomeric TG 18:2(9,12)_18:1(9)_18:0 species and an additional C=C positional isomer. Figure 4D shows MS/MS of m/z 919, which is analogous to the triolein single epoxidation product, and may also be attributed to the single epoxidation product of acyl chain and C=C positional isomers, structures of which are illustrated in Figure 4E. We make the following three observations by analyzing the lyso-diagnostic ion mass range from m/z 470−535, shown as inset (i) in Figure 4D, and the intact lipid diagnostic ion mass range from m/z 760−820, shown as inset (ii) in Figure 4D: (a) the peaks of highest intensity occur at m/z 477 and 493 in inset (i) and m/z 760 and 776 in inset (ii); (b) there are satellite peaks at ±2Da of these peaks; and (c) there are additional lower-intensity peaks emerging from the baseline that were not present in the standard solution of triolein. We attribute the high-intensity peaks to triolein lyso-form diagnostic ions ***1*** and ***2*** and intact-form diagnostic ions ***3*** and ***4***, which is expected due to the high expected natural abundance in EVOO as previously reported.[65] The satellite peaks and lower-intensity additional peaks provide structural elucidation of the positional isomers of TG 18:1(9)/18:1(9)/18:1(9), which are discussed below.

Initially, we consider the TG 18:2(9,12)_18:1(9)_18:0 acyl chain TG isomer (i.e., the middle structure of the three TG isomers shown in Figure 4E). The epoxidation and the successive fragmentation patterns of this isomer are described in Scheme S6. When considering this TG, epoxidation may occur at carbon 9 of the 18:2(9,12) acyl chain, the carbon 12 of the 18:2(9,12) acyl chain, or the carbon 9 of the 18:1(9) acyl chain. Additionally, when considering lyso-form diagnostic ions, the loss of each side chain must be considered since such fragmentation occurs nonselectively. Therefore, the loss of the 18:0 acyl chain, the 18:1 acyl chain, and the 18:2 acyl chain must be considered separately when determining lyso-form diagnostic ions as summarized in Scheme S6. This factor causes four diagnostic ions for each C=C position in the lyso-form alone, with two additional diagnostic ions per C=C from the intact form of the lipid, providing a total of six diagnostic ions corresponding to one C=C bond. Such complexity is beneficial for the attribution of diagnostic ions to a unique isomeric structure. However, we utilize the four highest-intensity diagnostic ions to support the presence of each isomer. In inset (i) of Figure 4D, lyso-form diagnostic ions ***17*** and ***18*** at m/z 517 and 533 are observed and attributed to the fragmentation of the single epoxidation at the carbon 12 location of the 18:2 side chain after the 18:0 acyl side chain is lost.

In inset (ii) of Figure 4D, intact-form diagnostic ions ***19*** and ***20*** at m/z 802 and 818 are observed and attributed to the fragmentation of the single epoxidation at the carbon 12 location of the 18:2 side chain. All other diagnostic ions corresponding to the TG 18:2(9,12)_18:1(9)_18:0 isomer (expected and observed) are summarized in Table S2B.

After fully characterizing the diagnostic ions possible from the epoxidation of the TG 18:2(9,12)_18:1(9)_18:0 acyl chain isomer, we noted that there were still a collection of peaks in both the lyso-form mass range and the intact-form mass range that were unaccounted for. We propose that these peaks are resultant from another C=C positional isomer of the TG 18:2(9,12)_18:1(9)_18:0 species with the 18:2(9,12) acyl chain replaced by a conjugated linoleic acid (CLA). This CLA acyl chain has C=C bonds at the carbon 10 and 12 locations (i.e., TG 18:2(10,12)_18:1(9)_18:0) as illustrated in the third isomeric structure shown in Figure 4E. We made this assignment based on the diagnostic ions observed in the MS/MS data. The list of full diagnostic ions possible from the epoxidation and fragmentation of this structure is shown in Scheme S7. Conjugated linoleic acids are naturally occurring positional isomers of linoleic acid and are prominent in the food industry and natural products.[67] Two specific CLA isomers, FA 18:2(9Z,11E) and FA 18:2(10E,12Z), are most abundant.[67] Although their structural differences are minimal, they have been shown to have different biological functions with the FA 18:2(9Z,11E) isomer being attributed to anticarcinogenic effects and the FA 18:2(10E,12Z) isomer being attributed to anti-obesity effects.[67−69] We propose the presence of the FA 18:2(10,12) CLA in the EVOO analyzed. This assignment is based on the presence of diagnostic ions ***21*** and ***22*** at m/z 491 and 507 in the stearic-loss lyso-form mass range and diagnostic ion ***24*** at m/z 792 in the intact-form mass range corresponding to the fragmentation of an epoxide at the 10E position of the CLA side chain.

As in the case of the TG 18:2(9, 12)_18:1(9)_18:0 isomer, all possible epoxidation sites and side chain losses to give the lyso-form were considered in Scheme S7. However, since the structural difference between the TG 18:2(9,12)_18:1(9)_18:0 isomer and the TG 18:2(10,12)_18:1(9)_18:0 isomer is small, we emphasize that the presence of the diagnostic ions related to epoxidation at the carbon 10 site provide evidence for this C=C positional isomer. We note that diagnostic ion ***23*** at m/z 776 is isobaric with a carbon 9 diagnostic ion of triolein. However, the presence of ***24*** in high abundance, along with the lyso-form diagnostic ions, supports the identification of the TG 18:2(10,12)_18:1(9)_18:0 isomer.

A full list of all diagnostic ions (expected and observed) related to this positional isomer is summarized in Table S2C. In sum, plasma-droplet fusing experiment enabled C=C positional analysis in the TG complex sample of EVOO to be elucidated. Based on this analysis, we have provided evidence for the presence of TG positional isomers not previously reported in EVOO samples. These results collectively showcase the power of the plasma-droplet reaction system enabled on the coaxial contained-ESI setup to provide lipid isomeric analysis at multiple levels, including the acyl chain and C=C positional isomer levels.

https://doi.org/10.1021/acsmeasuresciau.2c00051
ACS Meas. Sci. Au 2023, 3, 32−44

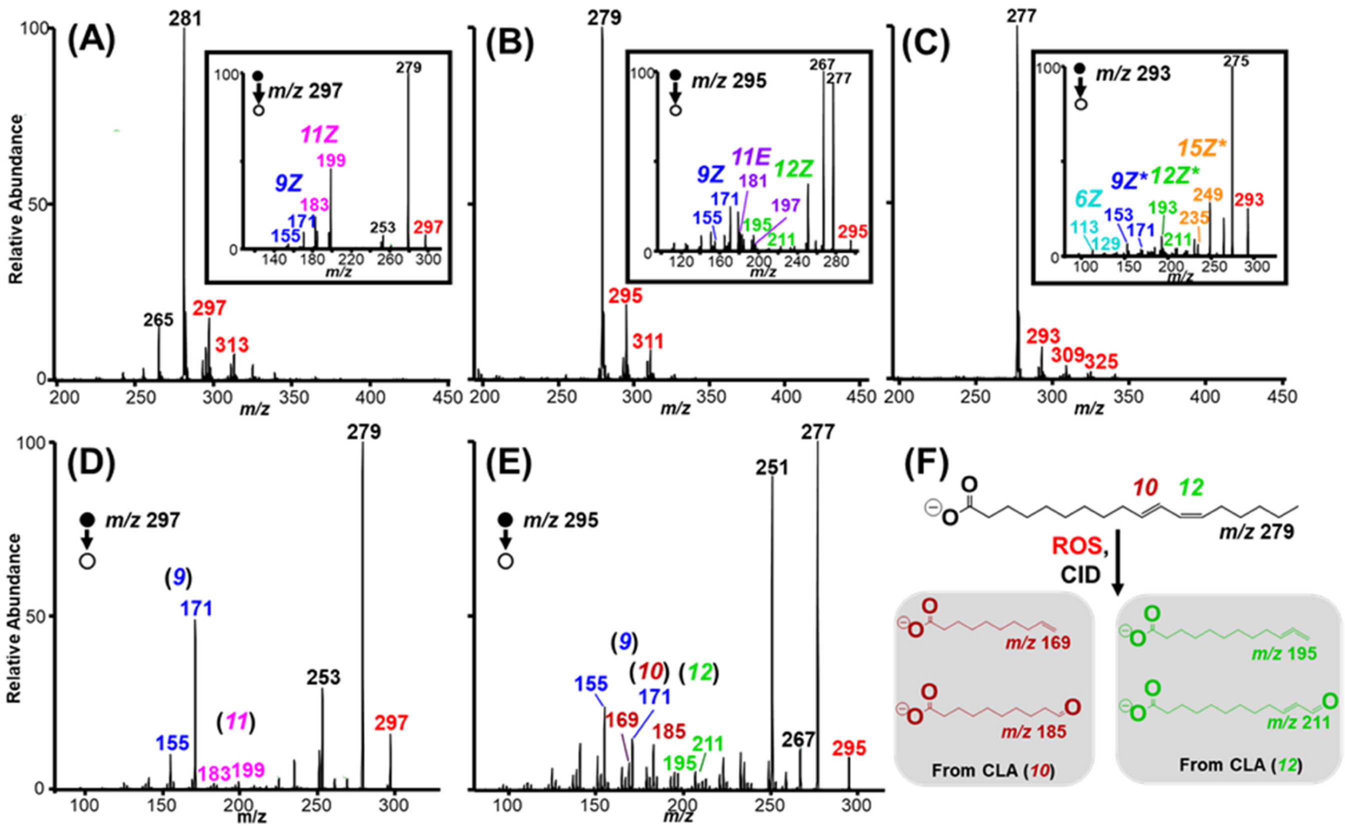

Figure 5. Negative-ion mode plasma-droplet contained-ESI MS analysis of (A) full mass spectrum of an isomeric mixture of free fatty acid standards oleic acid (18:1, 9Z) and *cis*-vaccenic acid (18:1, 11Z), with the Inset MS/MS showing CID of the single epoxide product at m/z 297 offering diagnostic ions for both isomers. (B) Full mass spectrum of standard mixture of linoleic acid (18:2, 9Z/12Z) and its conjugated linoleic acid (9Z/11E) isomer. The inset shows CID MS/MS of the single epoxide produce at m/z 295, revealing expected diagnostic ions for both isomers. (C) Full mass spectrum of standard isomeric mixture of α-linolenic acid (18:3, 9Z/12Z/15Z) and γ-linolenic acid (18:3, 6Z/9Z/12Z) with inset MS/MS of the single epoxide showing diagnostic ions for both isomers. (D) MS/MS of m/z 297 derived from analysis of the complex EVOO sample, which shows known diagnostic ions for FA 18:1(9) and FA 18:1(11) FAs. (E) MS/MS of m/z 295 derived from analysis of the complex EVOO sample showing diagnostic ions that confirm the presence of 18:2 (9,12) and 18:2 (10,12) side chain C═C positional isomers. (F) Reaction scheme highlighting diagnostic ions for the newly discovered FA 18:2 (10,12) C═C positional isomer.

Analysis of FAs and Isomeric Differentiation in Negative-Ion Mode

It is important to consider the hydrolysis of TGs to give substituent FAs as this is one process responsible for the total FA expression in a biological system. As demonstrated by others, FA expression, including the degree of unsaturation and position of C═C bonds, can give insight into the metabolic health of individuals and have implications in obesity, diabetes, and heart disease.[48] Thus, after demonstrating the use of the coaxial contained platform with etched silica capillaries for plasma-droplet fusing reactions of TGs for C═C positional analysis, we aimed to evaluate the emitter's capacity to perform isomeric mixture analysis of FAs. We perform FA analysis of the complex EVOO sample to determine if some of the exotic side chains identified (e.g., 18:2(10,12)) can be confirmed as FA released are a hydrolytic product from TGs. The analysis of the FAs also demonstrates the effectiveness of the plasma-droplet experiment in the negative-ion mode, thus covering both cathodic and anodic plasma generation during electrospray.

FA standards chosen include FA 18:1(9Z)—oleic acid, FA 18:2(9Z,12Z)—linoleic acid, and FA 18:3(9Z,12Z,15Z)—α-linolenic acid. These were selected because they are the FA analogues of the acyl chain compositions of triolein, trilinolein, and trilinolenin TG lipids, respectively. In addition to providing analogous double-bond configuration and demonstration of negative-ion mode analysis, these species were chosen (a) to allow fundamental study of the effect of C═C bond position on plasma-droplet-induced epoxidation reaction and (b) because natural occurring positional isomers of 18:1, 18:2, and 18:3 FAs are commercially available, furthering validation of the platform. For example, FA 18:1(11Z), *cis*-vaccenic acid, is a naturally occurring positional isomer to oleic acid with implications in human metabolic syndrome and kidney disease. The mixture of the two isomers presents a challenge to MS-based lipidomics since they have the same molecular weight (MW 282 Da). Cis-vaccenic acid has one C═C bond at the 11Z position as opposed to oleic acid with one C═C bond at the 9Z position. Isomeric differentiation of these species is possible using the epoxidation reaction performed in the plasma-droplet reaction in the contained-ES emitter. Figures S12A and S12B show the resultant spectra of oleic and *cis*-vaccenic acid, respectively, using Type I mode (no cavity) of the etched capillary emitter under optimized conditions. The full MS of the two isomers gives identical results with the main epoxidation product occurring at m/z 297, which is +16 Da away from the deprotonated $[M - H]^-$ ion at m/z 281. The MS/MS provides a unique mass spectral fingerprint for both isomers. Based on the expected CID epoxide fragmentation (Scheme S8), different product ions are

https://doi.org/10.1021/acsmeasuresciau.2c00051
ACS Meas. Sci. Au 2023, 3, 32−44

obtained for epoxidations occurring at different sites along the carbon backbone. The 9-carbon epoxide fragmentation gives MS/MS product ions m/z 155 and 171 (see inset in Figure S12A), which confirms the presence of oleic acid (18:1, 9Z). Similarly, the 11-carbon epoxide fragmentation products of *cis*-vaccenic acid (18:1, 11Z) are m/z 183 and 199 (see inset in Figure S12B). A 1:1 mixture of these positional isomers was made and analyzed with the contained-ES emitter to evaluate the ability to perform isomeric mixture analysis. The result of this experiment is shown in Figure 5A where the full MS again afforded the expected single 18:1 epoxidation product at m/z 297 with a contribution from the molecular oxygen addition at m/z 313. The inset MS/MS in Figure 5A was recorded after the fragmentation of the epoxide product (m/z 297), which registered both the expected 9Z diagnostic ions at m/z 155 and 171 indicating the presence of oleic acid, and the 11Z diagnostic ions at m/z 183 and 199 corresponding to *cis*-vaccenic acid.

Next, we evaluated linoleic acid, which is the fatty acid acyl chain in trilinolein, with unsaturation sites at the 9Z and 12Z positions. We compared its performance to the conjugated linoleic acid positional isomer with unsaturation at 9Z and 11E (i.e., FA 18:2(9Z,11E)). Figure S12C,D shows mass spectra corresponding to linoleic acid and the FA 18:2(9Z,11E) isomer, respectively. As expected, both full mass spectra give m/z 295 that corresponds to the epoxidation of one of the C=C bonds and m/z 311 that corresponds to the epoxidation of the two C=C bonds. CID MS/MS of linoleic acid (inset of Figure S12C) gives the four expected diagnostic ions (Scheme S8C) derived from fragmentation of the 9Z epoxide (m/z 155 and 171) and 12Z epoxide (m/z 195 and 211). Likewise, the inset in Figure S12D shows the MS/MS analysis of the FA 18:2(9Z,11E) positional isomer where the typical 9Z diagnostic ions were observed alongside the 11E diagnostic ions at m/z 181 and 197 (see details in Scheme S8D). Note: these analyses were based on the dissociation of the single epoxidation product (+O). The corresponding analysis of the double epoxidation product (+2O) at m/z 311 is provided in Figure S13, which also produces all expected diagnostic ions for both isomeric species. Analysis of a 1:1 (mole ratio) mixture of the two FA 18:2 isomers was performed, and the resultant mass spectra are displayed in Figure 5B. The full MS shows both the single and double epoxidation product at m/z 295 and 311, respectively. The inset MS/MS, however, clearly displays the 9Z diagnostic ions m/z 155 and 171 that originate from both species along with the 11E (m/z 181 and 197) and 12Z (m/z 195 and 211) diagnostic ions that are unique to linoleic acid and the conjugated linoleic acid isomer. See similar analysis for the double epoxidation product in Figure S14.

Finally, the commonly occurring ω-3 and ω-6 FA 18:3 isomers, α-linolenic and FA 18:3(6Z,9Z,12Z)—γ-linolenic acid, were evaluated in the plasma-droplet fusing reaction system using the contained-ES emitter. As stated previously, these ω-3 and ω-6 isomers have vast implications in human metabolic syndrome with high ω-6/ω-3 ratios promoting inflammation and lower ratios having a suppressive effect. The ω-3 18:3 FA evaluated here is α-linolenic acid with C=C bonds at the 9Z, 12Z, and 15Z positions. Here, the full MS analysis (Figure S12E) showed the single epoxidation product at m/z 293, the double epoxidation product at m/z 309, and the triple epoxidation at m/z 325 as supported by the inset MS/MS and expected epoxide CID fragmentation pattern (Scheme S8E). Diagnostic ions for C=C bond at 9Z and 12Z were similar to other FAs having the same C=C bond position as discussed above. Fragmentation at the 15Z site, however, was unique to the ω-3 18:3 FA and gave diagnostic ions at m/z 235 and 251. The MS/MS data (inset in Figure S12E) shows all expected diagnostic ions, except the appearance of the ion at m/z 249, which is 2 Da less than the expected diagnostic ion (m/z 251). We suggest a similar phenomenon to that observed in trilinolenin, where successive H_2 neutral loss via dehydrogenation occurs after the epoxide ring is subjected to collisional activation. The fact that the fragment ion at m/z 249 is related to the diagnostic ion at m/z 251 is validated in the MS/MS of the double epoxidation product shown in Figure S15A where the ion is clearly distinguished. Figure S15B shows the MS/MS of the triple epoxidation product of α-linolenic acid, which gives the same diagnostic ions as the single epoxidation product, however, with a more crowded baseline—likely due to contribution from molecular oxygen addition.

The ω-6 (FA 18:3) positional isomer, γ-linolenic acid, was also evaluated, and the results are summarized in Figure S12F. This species is unique to all others due to the C=C bond at the 6Z position. The single, double, and triple epoxidation products are observed in the full MS—occurring at the same m/z as the ω-3 isomer. However, the inset MS/MS in Figure S12F shows ions at m/z 133 and 129 which correspond to the expected CID fragmentation of the C=C bond at the 6Z site (see Scheme S8F for mechanistic interpretation of fragments). Other unsaturation sites of γ-linolenic acid occur at the 9Z and 12Z positions. The diagnostic ions expected from epoxide products at these sites are also unique due to the unsaturation at 6Z, causing them to be 2 Da lower than the 9Z and 12Z diagnostic ions of other FAs studied. We emphasize no convolution of these diagnostic ions with −2 Da dehydrogenation products that were sometimes observed for polyunsaturated acyl chains. This insight is based on the comparison of the ω-3 and ω-6 MS/MS data showing no such dehydrogenation in the ω-3 species. MS/MS data of the double and triple epoxidation fragment of γ-linolenic acid are shown in Figure S15C and S15D, respectively, which support the identification of all diagnostic ions.

Finally, a 1:1 mixture of the two FA 18:3 isomers was analyzed using the contained-ES emitter in Type I mode where the plasma and droplet fusion occurs on microseconds timescale. The resultant spectrum is shown in Figure 5C with the corresponding MS/MS analysis of the epoxide product at m/z 293 provided as inset. The 6Z and 12Z diagnostic ions are observed which support the presence of both isomers in solution as only α-linolenic acid has a 12Z C=C bond and only γ-linolenic has a 6Z C=C bond. The ion at m/z 249 (derived from the dehydrogenation of diagnostic ion m/z 251) is again observed. The importance of this ion is again supported by MS/MS of the double epoxide product of the isomeric mixture (Figure S16A) where m/z 251 is clearly distinguished. Structural analysis based on the triple epoxide product is shown in Figure S16B, which provides analogous diagnostic ions to the single epoxidation product.

Direct Analysis of FFAs in EVOO Complex Mixture

The principal reason for analyzing the standard fatty acids and their corresponding mixtures was to enable the application of the plasma-droplet reactions to identify FA components in EVOO in the negative-ion mode. Our expectation was that the

https://doi.org/10.1021/acsmeasuresciau.2c00051
ACS Meas. Sci. Au 2023, 3, 32−44

analysis of the FA components in EVOO will provide validation of the novel TG identified where the 18:2(10,12) side chain has replaced the 18:2(9,12) side chain in the naturally occurring TG 18:2_18:1_18:0 lipid. Simply put, we anticipated to detect FA 18:2(10,12) in EVOO. This expectation has been met.

To test this hypothesis, we performed negative-ion mode analysis on the EVOO complex sample where we recorded tandem MS on m/z 297 and 295, which corresponded to the single epoxidation of the 18:1 FA and 18:2 FA species, respectively. MS/MS of the peak at m/z 297 derived from the complex EVOO sample is shown in Figure 5D. This species fragmented via water and carbon dioxide losses, which could originate from both oleic and *cis*-vaccenic epoxide product. However, we detected intense peaks at m/z 155 and 171 attributable to fragmentation of the epoxide at the carbon 9 position in FA 18:1(9). Low-abundant peaks at m/z 183 and 199 were also observed, which likely originate from the fragmentation of the epoxide of the FA 18:1(11) isomer, which is known to have low natural abundance in EVOO. The MS/MS spectrum of the peak at m/z 295 corresponding to the epoxidation of the 18:2 FA species is shown in Figure 5E. Peaks at m/z 155 and 171 are again contributed to the fragmentation of an epoxide at the carbon 9 position of FA 18:2(9,12). Peaks at m/z 195 and 211 are contributed to the fragmentation of an epoxide at the carbon 12 position. The presence of additional peaks at m/z 169 and 185 are attributed to the FA 18:2(10,12) isomer, a summary of which is shown in Figure 5F. These provide validation for the novel TG species identified in positive-ion mode analysis of the EVOO sample.

■ CONCLUSIONS

A novel plasma-droplet reaction system was established on a coaxial contained-ES platform that utilized chemically etched silica capillaries to stabilize electrospray signal during the onset of corona discharge in positive- and negative-ion modes. The entrapment of reactive oxygen species from the discharge in the charged microdroplet created an oxidative environment that facilitated epoxidation reactions during the electrospray process. The coaxial spray mode utilized for this experiment enabled organic solvent not friendly for electrospray to be used for sensitive analysis of neutral triacylglyceride lipids after online mixing with droplets derived from aqueous ammonium acetate sprayed from etched capillary. This same coaxial spray capacity is expected to enable the coupling of the super reactive charged droplets derived from the plasma-droplet fusion mechanism on liquid chromatography−mass spectrometry systems for online modification of eluents.

In the current study, the fusion of plasma and charged droplets provided enhanced structural characterization of unsaturated triacylglyceride in extra virgin olive oil complex mixtures as validated through the analyses of multiple triglyceride standards. We used the platform to elucidate both acyl chain and C═C bond positional isomers. The novel quadruplet diagnostic fragment ions derived from the collision-induced dissociation of the lipid epoxides were used to confirm the presence of an acyl chain isomer of triolein in extra virgin olive oil. The same mode of fragmentation provided strong evidence for the existence of a C═C positional isomer, a triacylglyceride containing conjugated linoleic acid that has not been reported before. Negative-ion mode analysis of free fatty acids believed to have been hydrolyzed from the corresponding triacylglycerides in olive oil confirmed the presence of the conjugated linoleic acid as a highly potential acyl chain counterpart for some triglyceride isomers in the oil. Here too, we used standards of the expected free fatty acids to validate our tandem MS interpretations.

Lipid analysis is now part of routine blood tests and since human plasma contains many thousands of distinct/isomeric lipids, the importance of isomeric elucidation in lipidomics has been highlighted as a necessary step. This quest has resulted in widespread efforts to make such analyses possible and has incorporated offline derivatization and online methods involving instrumentation modifications that include liquid chromatography and ion mobility spectroscopy strategies. Based on the results of this study, we suggest the plasma-droplet fusing experiment in the coaxial contained-ES platform can provide a facile, accessible, and reliable method for C═C isomeric analysis on existing ion-trap mass spectrometers capable of conventional collision-induced dissociation. This new approach can represent a powerful tool in the ongoing efforts to overcome challenges to the field of lipidomics by enabling both shotgun and separation-based mass spectrometry lipidomics.

■ ASSOCIATED CONTENT

Supporting Information

The Supporting Information is available free of charge at https://pubs.acs.org/doi/10.1021/acsmeasuresciau.2c00051.

> Details of the experimental setup and optimization, chemical etching procedure, instrument, and materials; full reaction schemes for diagnostic ion determination and tandem MS data for TG and FA species with multiple epoxide products; and tables summarizing all diagnostic ions (PDF)

■ AUTHOR INFORMATION

Corresponding Author

Abraham K. Badu-Tawiah − *Department of Chemistry and Biochemistry, The Ohio State University, Columbus, Ohio 43210, United States;* orcid.org/0000-0001-8642-3431; Email: badu-tawiah.1@osu.edu

Authors

Alexander J. Grooms − *Department of Chemistry and Biochemistry, The Ohio State University, Columbus, Ohio 43210, United States*

Anna N. Nordmann − *Department of Chemistry and Biochemistry, The Ohio State University, Columbus, Ohio 43210, United States*

Complete contact information is available at: https://pubs.acs.org/10.1021/acsmeasuresciau.2c00051

Author Contributions

The manuscript was written through contributions of all authors. All authors have given approval to the final version of the manuscript.

Funding

This research was supported by the U.S. Department of Energy, Office of Basic Energy Sciences, Condensed Phase and Interfacial Molecular Science, under award number DE-SC0016044.

Notes

The authors declare no competing financial interest.

REFERENCES

(1) Wenk, M. R. Lipidomics: New Tools and Applications. *Cell* **2010**, *143*, 888−895.
(2) Blanksby, S. J.; Mitchell, T. W. Advances in Mass Spectrometry for Lipidomics. *Annu. Rev. Anal. Chem.* **2010**, *3*, 433−465.
(3) Yang, K.; Han, X. Lipidomics: Techniques, Applications, and Outcomes Related to Biomedical Sciences. *Trends Biochem. Sci.* **2016**, *41*, 954−969.
(4) Yang, K.; Cheng, H.; Gross, R. W.; Han, X. Automated Lipid Identification and Quantification by Multidimensional Mass Spectrometry-Based Shotgun Lipidomics. *Anal. Chem.* **2009**, *81*, 4356−4368.
(5) Yang, K.; Zhao, Z.; Gross, R. W.; Han, X. Shotgun Lipidomics Identifies a Paired Rule for the Presence of Isomeric Ether Phospholipid Molecular Species. *PLoS One* **2007**, *2*, No. e1368.
(6) Antonny, B. Mechanisms of Membrane Curvature Sensing. *Annu. Rev. Biochem.* **2011**, *80*, 101−123.
(7) Bigay, J.; Antonny, B. Curvature, Lipid Packing, and Electrostatics of Membrane Organelles: Defining Cellular Territories in Determining Specificity. *Dev. Cell* **2012**, *23*, 886−895.
(8) Manni, M. M.; Tiberti, M. L.; Pagnotta, S.; Barelli, H.; Gautier, R.; Antonny, B. Acyl Chain Asymmetry and Polyunsaturation of Brain Phospholipids Facilitate Membrane Vesiculation without Leakage. *eLife* **2018**, *7*, No. e34394.
(9) Ryhage, R.; Stenhagen, B. Mass Spectrometry in Lipid Research. *J. Lipid Res.* **1960**, *1*, 361−390.
(10) Hites, R. A. [44] Mass Spectrometry of Triglycerides. In *Methods in Enzymology; Lipids Part B*; Academic Press, 1975; Vol. 35, pp 348−359.
(11) Hsu, F.-F.; Turk, J. Structural Characterization of Triacylglycerols as Lithiated Adducts by Electrospray Ionization Mass Spectrometry Using Low-Energy Collisionally Activated Dissociation on a Triple Stage Quadrupole Instrument. *J. Am. Soc. Mass Spectrom.* **1999**, *10*, 587−599.
(12) Reshef, L.; Olswang, Y.; Cassuto, H.; Blum, B.; Croniger, C. M.; Kalhan, S. C.; Tilghman, S. M.; Hanson, R. W. Glyceroneogenesis and the Triglyceride/Fatty Acid Cycle *. *J. Biol. Chem.* **2003**, *278*, 30413−30416.
(13) Yen, C.-L. E.; Stone, S. J.; Koliwad, S.; Harris, C.; Farese, R. V. Thematic Review Series: Glycerolipids. DGAT Enzymes and Triacylglycerol Biosynthesis. *J. Lipid Res.* **2008**, *49*, 2283−2301.
(14) Kennedy, E. P. Metabolism of Lipides. *Annu. Rev. Biochem.* **1957**, *26*, 119−148.
(15) Coleman, R. Enzymes of Triacylglycerol Synthesis and Their Regulation. *Prog. Lipid Res.* **2004**, *43*, 134−176.
(16) Coleman, R. A.; Lewin, T. M.; Van Horn, C. G.; Gonzalez-Baró, M. R. Do Long-Chain Acyl-CoA Synthetases Regulate Fatty Acid Entry into Synthetic Versus Degradative Pathways? *J. Nutr.* **2002**, *132*, 2123−2126.
(17) Kayden, H. J.; Senior, J. R.; Mattson, F. H. The Monoglyceride Pathway of Fat Absorption in Man*. *J. Clin. Invest.* **1967**, *46*, 1695−1703.
(18) Mansbach, C. M.; Gorelick, F. Development and Physiological Regulation of Intestinal Lipid Absorption. II. Dietary Lipid Absorption, Complex Lipid Synthesis, and the Intracellular Packaging and Secretion of Chylomicrons. *Am. J. Physiol.: Gastrointest. Liver Physiol.* **2007**, *293*, G645−G650.
(19) Schulze, P. C. Myocardial Lipid Accumulation and Lipotoxicity in Heart Failure1. *J. Lipid Res.* **2009**, *50*, 2137−2138.
(20) Wahba, I. M.; Mak, R. H. Obesity and Obesity-Initiated Metabolic Syndrome: Mechanistic Links to Chronic Kidney Disease. *Clin. J. Am. Soc. Nephrol.* **2007**, *2*, 550−562.
(21) Unger, R. H. Lipotoxic Diseases. *Annu. Rev. Med.* **2002**, *53*, 319−336.
(22) Moller, D. E.; Kaufman, K. D. Metabolic Syndrome: A Clinical and Molecular Perspective. *Annu. Rev. Med.* **2005**, *56*, 45−62.
(23) Accioly, M. T.; Pacheco, P.; Maya-Monteiro, C. M.; Carrossini, N.; Robbs, B. K.; Oliveira, S. S.; Kaufmann, C.; Morgado-Diaz, J. A.; Bozza, P. T.; Viola, J. P. Lipid Bodies Are Reservoirs of Cyclooxygenase-2 and Sites of Prostaglandin-E2 Synthesis in Colon Cancer Cells. *Cancer Res.* **2008**, *68*, 1732−1740.
(24) Liu, Y. Fatty Acid Oxidation Is a Dominant Bioenergetic Pathway in Prostate Cancer. *Prostate Cancer Prostatic Dis.* **2006**, *9*, 230−234.
(25) Khasawneh, J.; Schulz, M. D.; Walch, A.; Rozman, J.; Angelis, M. H.; de Klingenspor, M.; Buck, A.; Schwaiger, M.; Saur, D.; Schmid, R. M.; Klöppel, G.; Sipos, B.; Greten, F. R.; Arkan, M. C. Inflammation and Mitochondrial Fatty Acid β-Oxidation Link Obesity to Early Tumor Promotion. *Proc. Natl. Acad. Sci. U.S.A.* **2009**, *106*, 3354−3359.
(26) Samudio, I.; Harmancey, R.; Fiegl, M.; Kantarjian, H.; Konopleva, M.; Korchin, B.; Kaluarachchi, K.; Bornmann, W.; Duvvuri, S.; Taegtmeyer, H.; Andreeff, M. Pharmacologic Inhibition of Fatty Acid Oxidation Sensitizes Human Leukemia Cells to Apoptosis Induction. *J. Clin. Invest.* **2010**, *120*, 142−156.
(27) Pike, L. S.; Smift, A. L.; Croteau, N. J.; Ferrick, D. A.; Wu, M. Inhibition of Fatty Acid Oxidation by Etomoxir Impairs NADPH Production and Increases Reactive Oxygen Species Resulting in ATP Depletion and Cell Death in Human Glioblastoma Cells. *Biochim. Biophys. Acta, Bioenerg.* **2011**, *1807*, 726−734.
(28) Simopoulos, A. P. The Importance of the Ratio of Omega-6/Omega-3 Essential Fatty Acids. *Biomed. Pharmacother.* **2002**, *56*, 365−379.
(29) Simopoulos, A. P. Evolutionary Aspects of Diet, the Omega-6/Omega-3 Ratio and Genetic Variation: Nutritional Implications for Chronic Diseases. *Biomed. Pharmacother.* **2006**, *60*, 502−507.
(30) Allayee, H.; Roth, N.; Hodis, H. N. Polyunsaturated Fatty Acids and Cardiovascular Disease: Implications for Nutrigenetics. *Lifestyle Genomics* **2009**, *2*, 140−148.
(31) Simopoulos, A. P. An. Increase in the Omega-6/Omega-3 Fatty Acid Ratio Increases the Risk for Obesity. *Nutrients* **2016**, *8*, 128.
(32) Swanson, D.; Block, R.; Mousa, S. A. Omega-3 Fatty Acids EPA and DHA: Health Benefits Throughout Life. *Adv. Nutr.* **2012**, *3*, 1−7.
(33) Vriens, K.; Christen, S.; Parik, S.; Broekaert, D.; Yoshinaga, K.; Talebi, A.; Dehairs, J.; Escalona-Noguero, C.; Schmieder, R.; Cornfield, T.; Charlton, C.; Romero-Pérez, L.; Rossi, M.; Rinaldi, G.; Orth, M. F.; Boon, R.; Kerstens, A.; Kwan, S. Y.; Faubert, B.; Méndez-Lucas, A.; Kopitz, C. C.; Chen, T.; Fernandez-Garcia, J.; Duarte, J. A. G.; Schmitz, A. A.; Steigemann, P.; Najimi, M.; Hägebarth, A.; Van Ginderachter, J. A.; Sokal, E.; Gotoh, N.; Wong, K.-K.; Verfaillie, C.; Derua, R.; Munck, S.; Yuneva, M.; Beretta, L.; DeBerardinis, R. J.; Swinnen, J. V.; Hodson, L.; Cassiman, D.; Verslype, C.; Christian, S.; Grünewald, S.; Grünewald, T. G. P.; Fendt, S.-M. Evidence for an Alternative Fatty Acid Desaturation Pathway Increasing Cancer Plasticity. *Nature* **2019**, *566*, 403−406.
(34) Thomas, M. C.; Mitchell, T. W.; Harman, D. G.; Deeley, J. M.; Nealon, J. R.; Blanksby, S. J. Ozone-Induced Dissociation: Elucidation of Double Bond Position within Mass-Selected Lipid Ions. *Anal. Chem.* **2008**, *80*, 303−311.
(35) Poad, B. L. J.; Pham, H. T.; Thomas, M. C.; Nealon, J. R.; Campbell, J. L.; Mitchell, T. W.; Blanksby, S. J. Ozone-Induced Dissociation on a Modified Tandem Linear Ion-Trap: Observations of Different Reactivity for Isomeric Lipids. *J. Am. Soc. Mass Spectrom.* **2010**, *21*, 1989−1999.
(36) Marshall, D. L.; Pham, H. T.; Bhujel, M.; Chin, J. S. R.; Yew, J. Y.; Mori, K.; Mitchell, T. W.; Blanksby, S. J. Sequential Collision- and Ozone-Induced Dissociation Enables Assignment of Relative Acyl Chain Position in Triacylglycerols. *Anal. Chem.* **2016**, *88*, 2685−2692.
(37) Campbell, J. L.; Baba, T. Near-Complete Structural Characterization of Phosphatidylcholines Using Electron Impact Excitation of Ions from Organics. *Anal. Chem.* **2015**, *87*, 5837−5845.
(38) Williams, P. E.; Klein, D. R.; Greer, S. M.; Brodbelt, J. S. Pinpointing Double Bond and Sn -Positions in Glycerophospholipids

via Hybrid 193 Nm Ultraviolet Photodissociation (UVPD) Mass Spectrometry. *J. Am. Chem. Soc.* **2017**, *139*, 15681−15690.
(39) Ma, X.; Xia, Y. Pinpointing Double Bonds in Lipids by Paternò-Büchi Reactions and Mass Spectrometry. *Angew. Chem., Int. Ed.* **2014**, *53*, 2592−2596.
(40) Ma, X.; Chong, L.; Tian, R.; Shi, R.; Hu, T. Y.; Ouyang, Z.; Xia, Y. Identification and Quantitation of Lipid C═C Location Isomers: A Shotgun Lipidomics Approach Enabled by Photochemical Reaction. *Proc. Natl. Acad. Sci. U.S.A.* **2016**, *113*, 2573−2578.
(41) Zhang, W.; Chiang, S.; Li, Z.; Chen, Q.; Xia, Y.; Ouyang, Z. A Polymer Coating Transfer Enrichment Method for Direct Mass Spectrometry Analysis of Lipids in Biofluid Samples. *Angew. Chem., Int. Ed.* **2019**, *58*, 6064−6069.
(42) Esch, P.; Heiles, S. Investigating C═C Positions and Hydroxylation Sites in Lipids Using Paternò−Büchi Functionalization Mass Spectrometry. *Analyst* **2020**, *145*, 2256−2266.
(43) Xia, T.; Yuan, M.; Xu, Y.; Zhou, F.; Yu, K.; Xia, Y. Deep Structural Annotation of Glycerolipids by the Charge-Tagging Paterno−Büchi Reaction and Supercritical Fluid Chromatography−Ion Mobility Mass Spectrometry. *Anal. Chem.* **2021**, *93*, 8345−8353.
(44) Thomas, M. C.; Mitchell, T. W.; Blanksby, S. J. OnLine Ozonolysis Methods for the Determination of Double Bond Position in Unsaturated Lipids. In Lipidomics: Volume 1: Methods and Protocols. In *Methods in Molecular Biology* Armstrong, D., Ed.; Humana Press: Totowa, NJ, 2009; pp 413−441.
(45) Feng, Y.; Chen, B.; Yu, Q.; Li, L. Identification of Double Bond Position Isomers in Unsaturated Lipids by m -CPBA Epoxidation and Mass Spectrometry Fragmentation. *Anal. Chem.* **2019**, *91*, 1791−1795.
(46) Cao, W.; Ma, X.; Li, Z.; Zhou, X.; Ouyang, Z. Locating Carbon−Carbon Double Bonds in Unsaturated Phospholipids by Epoxidation Reaction and Tandem Mass Spectrometry. *Anal. Chem.* **2018**, *90*, 10286−10292.
(47) Bouza, M.; Li, Y.; Wang, A. C.; Wang, Z. L.; Fernández, F. M. Triboelectric Nanogenerator Ion Mobility−Mass Spectrometry for In-Depth Lipid Annotation. *Anal. Chem.* **2021**, *93*, 5468−5475.
(48) Swiner, D. J.; Kulyk, D. S.; Osae, H.; Durisek, G. R., III; Badu-Tawiah, A. K. Reactive Thread Spray Mass Spectrometry for Localization of C═C Bonds in Free Fatty Acids: Applications for Obesity Diagnosis. *Anal. Chem.* **2022**, *94*, 2358−2365.
(49) Guo, Y.; Li, S.; Wu, Z.; Zhu, K.; Han, Y.; Wang, N. Interaction between Electrospray Using Ionic Liquid and Simultaneous Corona Discharge under Positive and Negative Polarity. *Phys. Plasmas* **2019**, *26*, No. 073511.
(50) Miller, C. F.; Kulyk, D. S.; Kim, J. W.; Badu-Tawiah, A. K. Re-Configurable, Multi-Mode Contained-Electrospray Ionization for Protein Folding and Unfolding on the Millisecond Time Scale. *Analyst* **2017**, *142*, 2152−2160.
(51) Miller, C. F.; Burris, B. J.; Badu-Tawiah, A. K. Spray Mechanism of Contained-Electrospray Ionization. *J. Am. Soc. Mass Spectrom.* **2020**, *31*, 1499−1508.
(52) Sahraeian, T.; Kulyk, D. S.; Badu-Tawiah, A. K. Droplet Imbibition Enables Nonequilibrium Interfacial Reactions in Charged Microdroplets. *Langmuir* **2019**, *35*, 14451−14457.
(53) Kelly, R. T.; Page, J. S.; Luo, Q.; Moore, R. J.; Orton, D. J.; Tang, K.; Smith, R. D. Chemically Etched Open Tubular and Monolithic Emitters for Nanoelectrospray Ionization Mass Spectrometry. *Anal. Chem.* **2006**, *78*, 7796−7801.
(54) Kulyk, D. S.; Swiner, D. J.; Sahraeian, T.; Badu-Tawiah, A. K. Direct Mass Spectrometry Analysis of Complex Mixtures by Nanoelectrospray with Simultaneous Atmospheric Pressure Chemical Ionization and Electrophoretic Separation Capabilities. *Anal. Chem.* **2019**, *91*, 11562−11568.
(55) Kulyk, D. S.; Sahraeian, T.; Wan, Q.; Badu-Tawiah, A. K. Reactive Olfaction Ambient Mass Spectrometry. *Anal. Chem.* **2019**, *91*, 6790−6799.
(56) Suga, Y.; Sekiguchi, H. Epoxidation of Carbon Double Bond Using Atmospheric Non-Equilibrium Oxygen Plasma. *Thin Solid Films* **2006**, *506−507*, 427−431.
(57) Chintalapudi, K.; K Badu-Tawiah, A. An Integrated Electrocatalytic NESI-MS Platform for Quantification of Fatty Acid Isomers Directly from Untreated Biofluids. *Chem. Sci.* **2020**, *11*, 9891−9897.
(58) Thomas, M. C.; Mitchell, T. W.; Blanksby, S. J. Ozonolysis of Phospholipid Double Bonds during Electrospray Ionization: A New Tool for Structure Determination. *J. Am. Chem. Soc.* **2006**, *128*, 58−59.
(59) Murphy, R. C.; James, P. F.; McAnoy, A. M.; Krank, J.; Duchoslav, E.; Barkley, R. M. Detection of the Abundance of Diacylglycerol and Triacylglycerol Molecular Species in Cells Using Neutral Loss Mass Spectrometry. *Anal. Biochem.* **2007**, *366*, 59−70.
(60) Zheng, L.; T'Kind, R.; Decuypere, S.; von Freyend, S. J.; Coombs, G. H.; Watson, D. G. Profiling of Lipids in Leishmania Donovani Using Hydrophilic Interaction Chromatography in Combination with Fourier Transform Mass Spectrometry. *Rapid Commun. Mass Spectrom.* **2010**, *24*, 2074−2082.
(61) Burris, B. J.; Badu-Tawiah, A. K. Enzyme-Catalyzed Hydrolysis of Lipids in Immiscible Microdroplets Studied by Contained-Electrospray Ionization. *Anal. Chem.* **2021**, *93*, 13001−13007.
(62) Heiss, D. R.; Badu-Tawiah, A. K. In-Source Microdroplet Derivatization Using Coaxial Contained-Electrospray Mass Spectrometry for Enhanced Sensitivity in Saccharide Analysis. *Anal. Chem.* **2021**, *93*, 16779−16786.
(63) Lee, J. K.; Kim, S.; Nam, H. G.; Zare, R. N. Microdroplet Fusion Mass Spectrometry for Fast Reaction Kinetics. *Proc. Natl. Acad. Sci. U.S.A.* **2015**, *112*, 3898−3903.
(64) Venter, A.; Sojka, P. E.; Cooks, R. G. Droplet Dynamics and Ionization Mechanisms in Desorption Electrospray Ionization Mass Spectrometry. *Anal. Chem.* **2006**, *78*, 8549−8555.
(65) Gómez-Ariza, J.; Arias-Borrego, A.; García-Barrera, T.; Beltran, R. Comparative Study of Electrospray and Photospray Ionization Sources Coupled to Quadrupole Time-of-Flight Mass Spectrometer for Olive Oil Authentication. *Talanta* **2006**, *70*, 859−869.
(66) da Silveira, R.; Vágula, J. M.; de Lima Figueiredo, I.; Claus, T.; Galuch, M. B.; Santos Junior, O. O.; Visentainer, J. V. Rapid Methodology via Mass Spectrometry to Quantify Addition of Soybean Oil in Extra Virgin Olive Oil: A Comparison with Traditional Methods Adopted by Food Industry to Identify Fraud. *Food Res. Int.* **2017**, *102*, 43−50.
(67) Subbaiah, P. V.; Sircar, D.; Aizezi, B.; Mintzer, E. Differential Effects of Conjugated Linoleic Acid Isomers on the Biophysical and Biochemical Properties of Model Membranes. *Biochim. Biophys. Acta, Biomembr.* **2010**, *1798*, 506−514.
(68) Pariza, M. W. Perspective on the Safety and Effectiveness of Conjugated Linoleic Acid. *Am. J. Clin. Nutr.* **2004**, *79*, 1132S−1136S.
(69) Belury, M. A. Dietary Conjugated Linoleic Acid In Health: Physiological Effects and Mechanisms of Action. *Annu. Rev. Nutr.* **2002**, *22*, 505−531.

https://doi.org/10.1021/acsmeasuresciau.2c00051
ACS Meas. Sci. Au 2023, 3, 32−44